PROCEEDINGS, 47th Workshop on Geothermal Reservoir Engineering
Stanford University, Stanford, California, February 7-9, 2022
SGP-TR-223

Monitoring Geothermal Flow at the Lightning Dock Geothermal Area, New Mexico Using Long-Duration Passive Seismic Imaging

Kai Gao[1], Lianjie Huang[1], Joel Edwards[2], Trenton Cladouhos[3]

[1]Los Alamos National Laboratory, Los Alamos, NM 87545, USA

[2]Zanskar Geothermal, 2365 Mountain Vista Lane Ste 5, Provo, UT 84606, USA

[3]Cyrq Energy, Inc., 4010 Stone Way North, Suite 400, Seattle, WA 98103, USA

Keywords: long-period long-duration signals, passive seismic imaging, geothermal fluid flow, geothermal fracture system

ABSTRACT

Monitoring subsurface fluid flow is crucial for optimizing geothermal energy production. The Lightning Dock Geothermal field (LDG) is located on the east side of Animas Valley in Hidalgo County, New Mexico, USA. LDG geothermal wells produce from fractures within the intersection of buried normal faults, as revealed by drilling and previous seismic traveltime tomography and gravity inversion. During July to August, 2020, Zanskar deployed a large-N nodal array consisting of 1,206 seismic geophones centered around the LDG production and injection region to acquire continuous passive seismic data. We first update the velocity model using an adjoint-state first-arrival traveltime tomography using several borehole string shot data acquired at LDG. We then apply a frequency-domain full-wavefield passive seismic imaging method to the acquired long-duration passive seismic data to image the subsurface fluid-flow pathways at LDG and their temporal changes. Our tomography and passive imaging results reveal high-resolution time-lapse geothermal fluid pathway images at LDG. We analyze the temporal-spatial relationships between the imaged flow pathways and geothermal production activities at LDG using these imaging results. Our imaging results provide valuable information for understanding the geothermal resource and current fluid pathways and **FOR** siting new wells at LDG.

1. INTRODUCTION

The Lightning Dock geothermal (LDG) power generating station is located in the Animas Valley, Hidalgo County, New Mexico, which ranges approximately 11 to 21 km in width and approximately 145 km in length. The geothermal area lies at the foot of the Pyramid Mountains which border the Animas Valley in the east (see Figure 1). The primary geological structures of the area contain a north-trending basin and range features and a caldera ring fracture zone. The LDG power station is a binary geothermal power plant.

Three major regional tectonic features enclose the Lightning Dock geothermal system: a mid-Tertiary caldera ring fracture zone, a major basement structure zone, and a young incipient normal fault tip. The upflow zone is due to the intrusion of the mid-Tertiary caldera ring fracture in the horst block of the normal fault system. The structure of the LDG geothermal anomaly is controlled by the north-south trending Animas Fault (see Figure 2), which has a 500 m displacement on average, and by the Muir Cauldron, which formed in the mid-Tertiary and intersects with the Animas Fault. The Animas Fault ends at the northern boundary of the LDG geothermal anomaly, and may have enhanced the local fracture permeability. The LDG reservoir is approximately 2.5 km long from north to south, and 1.5 km wide from east to west. The reservoir depth is 25 m on the north end of the anomaly, and 200 m at the south end, with a approximate volume of 0.66 km . Previous studies showed that there are two relatively shallow conventional reservoirs of moderate temperature at depths 1,200 and 3,300 ft, as well as an enhanced geothermal system type reservoir at the depths 3,000 to 4,000 ft. The reservoirs within the geothermal anomaly are recharged primarily by mountain front water drainage.

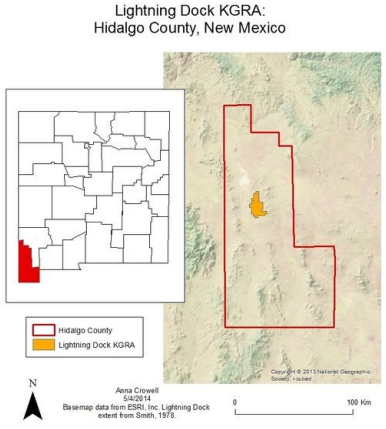

Figure 1: Location of the Lightning Dock power generating station in New Mexico, USA. The red-lined region indicates the Hildago County, NM, and the yellow-colored highlighted region is the LDG area.

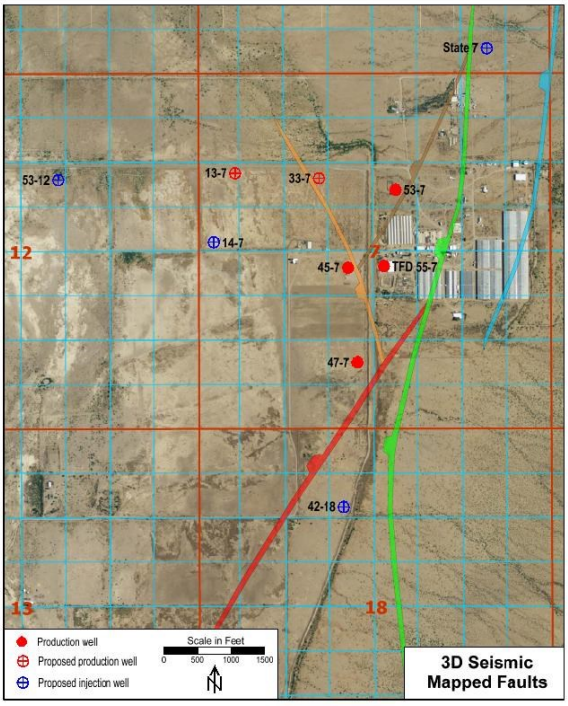

Figure 2: A map view of the major geological faults (red, green, and orange colored curves) at the LDG resource area mapped by our industrial collaborator.

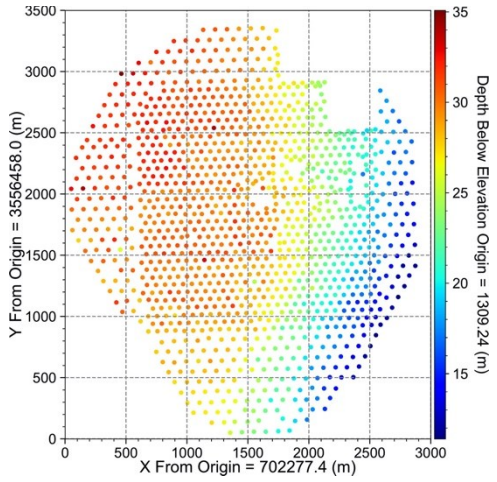

Figure 3: The distribution of large-N nodal geophones used in the LDG passive seismic survey conducted by Zanskar.

During July 27 to August 19, 2020, Zanskar deployed and operated a large-N array consisting of 1,206 nodal geophones at the LDG resource area to image the geothermal reservoirs and its fluid-flow pathways using continuous passive seismic data, thus to facilitate placing new injection wells. Figure 3 displays the distribution of these nodal geophones at the LDG resource area. According to the operation logs and the project report of Zanskar (Zanskar, 2021), there were several activities at the LDG area overlapping with the continuous data acquisition period, including a scheduled power plant outage (July 24 to August 5); a wash, ream and acid frac stimulation at well 47-7 (August 11 to 19); an injection test at well 53-7 (August 10 to 11); and a deployment of seven string shots at various depths in wells 17-7 and 63-7 (August 14 to 15). The seven string shots and their first-arrival arrival traveltimes recorded at the large-N array were used to produce a starting, smooth P-wave velocity (Vp) model using ray tomography by Zanskar. Zanskar's tomography result reveals LDG's horst and graben structure and the basin-bounding normal faults that may be associated with the geothermal reservoir. Zanskar found that the updated velocity model improves fluid-flow pathway passive seismic imaging.

Long-period long-duration (LPLD) seismic events are relatively low-amplitude signals that have been observed in, for example, hydraulic fracturing in shale-gas and tight-gas reservoirs (Das and Zoback, 2013), volcano tremors (Yukutake et al., 2017), and geothermal reservoirs. In geothermal exploration, LPLD signals are usually associated with the interaction between geothermal fluid flow and geothermal fracture pathways. The flow through fractures and possible induced fracture expansion and contraction behave as long-time tremor-like microseismic sources. Imaging the geothermal flow activity and the associated fracture pathways using these passive seismic signals is effectively equivalent to locating microseismic sources.

We first update the initial velocity model obtained by Zanskar using adjoint-state first-arrival traveltime tomography (FATT) of seven borehole string shots data, and then use the LPLD signals recorded at LDG to perform full-wavefield-based passive seismic imaging to image the fluid flow activities. Our passive imaging reveals the time-lapse changes of geothermal fluid flow activities at the LDG resource area over a period of 21 days.

2. METHDOLOGY

Rather than using traveltime-based passive seismic imaging methods, we use full-wavefield-based passive seismic imaging methods to image the geothermal fluid flow activities and the geothermal fracture pathways. One of the fundamental approaches for full-wavefield passive seismic imaging is zero-lag auto-correlation time-reversal imaging (Artman et al., 2010; Liu et al., 2020):

$$I(x) = \sum_{\omega} W^{*}(x,\omega)W(x,\omega), \tag{1}$$

where $\boldsymbol{\omega}$ is the angular frequency, $\boldsymbol{I(x)}$ is the source image at spatial location $\boldsymbol{x}$, and $\boldsymbol{W(x,\omega)}$ is the frequency-domain wavefield expressed as

$$W(x,\omega) = \sum_{i=1}^{N_r} G^{*}(x_i,x,\omega)D(x_i,\omega), \tag{2}$$

where $G(x_i,x,\omega)$ is Green's function at angular frequency $\boldsymbol{\omega}$ associated with the $\boldsymbol{i}$-th seismic station, $\boldsymbol{D}(x_i,\omega)$ is the passive seismic data in the frequency domain associated with the $\boldsymbol{i}$-th seismic station, and the superscript "$*$" represents the complex conjugate.

To improve the accuracy of the source image produced using the full-wavefield time-reversal imaging framework, we adopt an improved version of the above zero-lag auto-correlation passive seismic imaging method, the cross-coherence seismic migration method (Liu et al., 2020) to image the geothermal flow activities using the LDLP signals. In cross-coherence migration, the source image is produced using

$$I(x) = \sum_{\omega}\sum_{i=1}^{N_r} G(x_i,x,\omega)\frac{D^{*}(x_i,\omega)}{|D(x_i,\omega)|}\sum_{j=1}^{N_r} G(x_j,x,\omega)\frac{D(x_j,\omega)}{|D(x_j,\omega)|}, \tag{3}$$

In our implementation, we first compute the frequency-domain wavefields $W(x,\omega)$ using a discrete Fourier transform method (Sirgue et al., 2008) based on a time-domain wave equation solver, and then compute the source images for the continuously recorded passive seismic data recorded at the large-N array for different days of the passive seismic survey.

3. RESULTS

Full-wavefield-based passive seismic imaging methods, including the cross-coherence seismic migration method we use for imaging geothermal fluid flow pathways based on LPLD signals, generally require an accurate velocity model for the wavefield to be properly focused to their actual excitation location.

An active-source seismic survey was performed by exciting a total of seven string shots in existing geothermal wells at the LDG resource area and acquiring seismic data using the surface large-N array. Figure 4 displays the picked traveltime associated with this string-shot survey. A smooth Vp model displayed in Figure 6 was then derived using ray tomography by Zanskar.

The most evident geological feature revealed by this tomography-derived model is a fault (Animas Fault) orienting in the north-south direction. The geological block to the east of the fault has a higher velocity than that to the west of the fault, and the velocity different can be as high as 3,000 m/s.

Based on this ray-tomography-derived velocity model, we perform a 3D FATT (Taillandier et al., 2009) using the traveltimes picked from the string-shot common-shot gathers. We display the inverted Vp model in Figure 6. Compared with the initial velocity model in Figure 5, we find that the FATT-updated velocity model is of higher spatial resolution. The region around the Animas Fault shows more heterogeneities that are missing in the initial ray-tomography model.

Our 3D FATT also leads to improved matching between the synthetic and the observed string-shot traveltimes. Figure 7 shows the difference between the synthetic and the observed traveltimes in the original Vp model. It is evident that in the original Vp model, the synthetic traveltimes are generally shorter than the observed traveltimes, meaning that the original model may contain overall higher than actual velocity values. By contrast, Figure 8 shows the difference between the synthetic and the observed traveltimes in the FATT-updated Vp model. We observe that in all seven string-shot common-shot gathers, the traveltime misfits are notably reduced to values around zero in the updated velocity model.

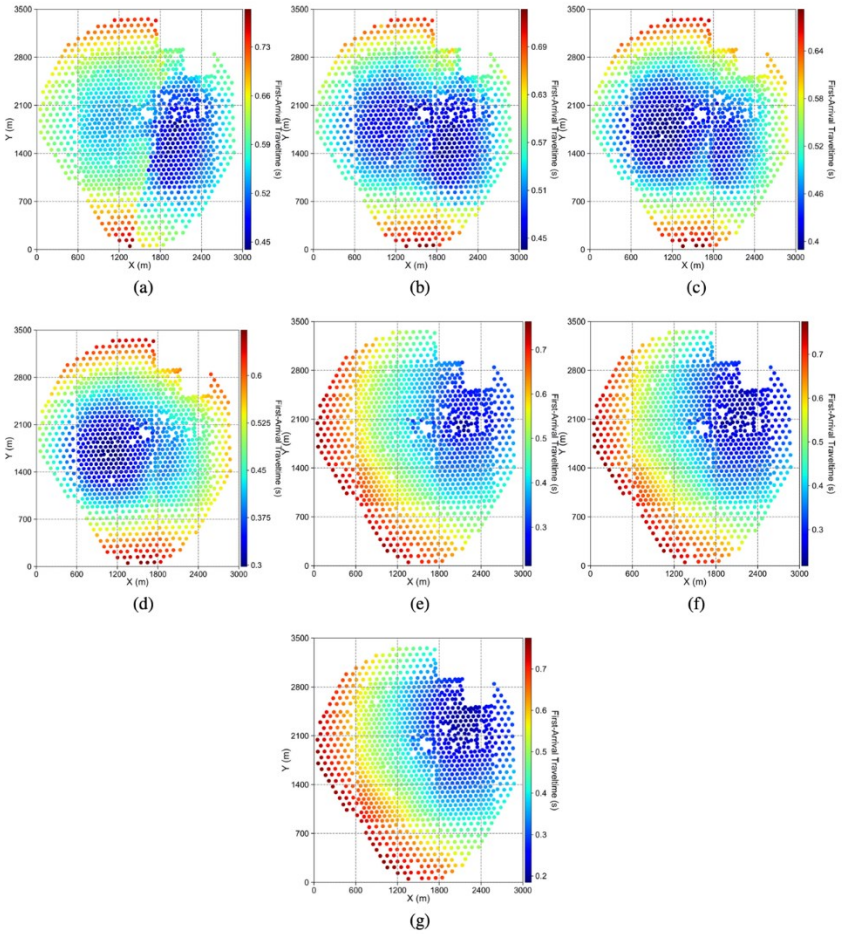

Figure 4: Panels (a)-(g) display the first-arrival traveltimes picked by Zanskar from the data of seven string shots.

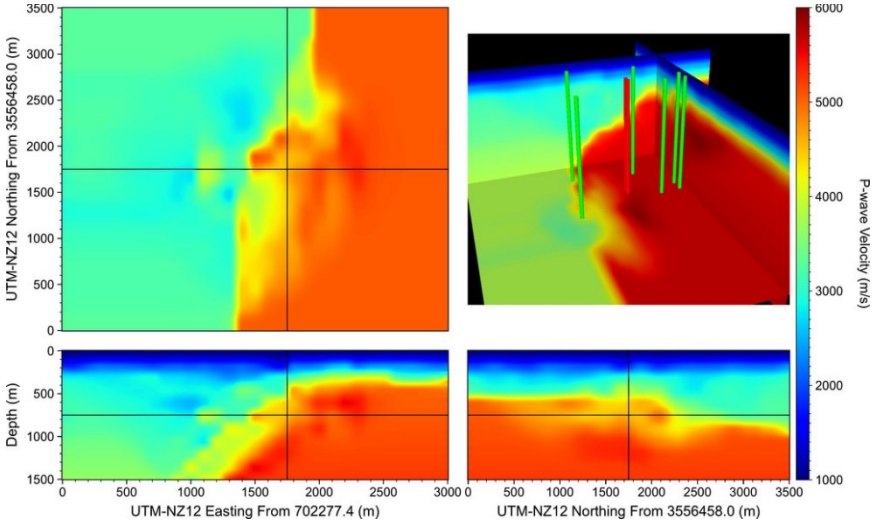

Figure 5: The P-wave velocity model obtained using ray tomography by Zanskar. The green tubes are active injection wells, and the red tubes are active geothermal production wells.

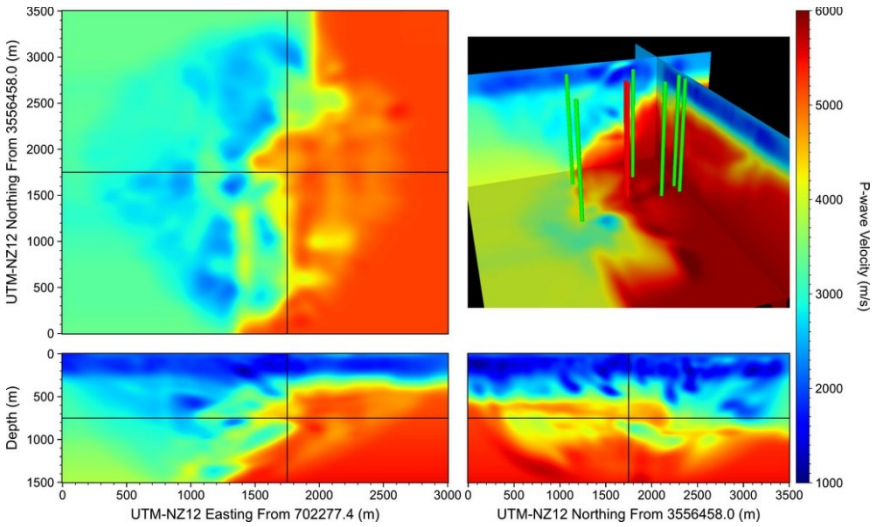

Figure 6: The P-wave velocity model obtained using LANL's adjoint-state FATT based on the first-arrival traveltime picks on the data of the seven string shots.

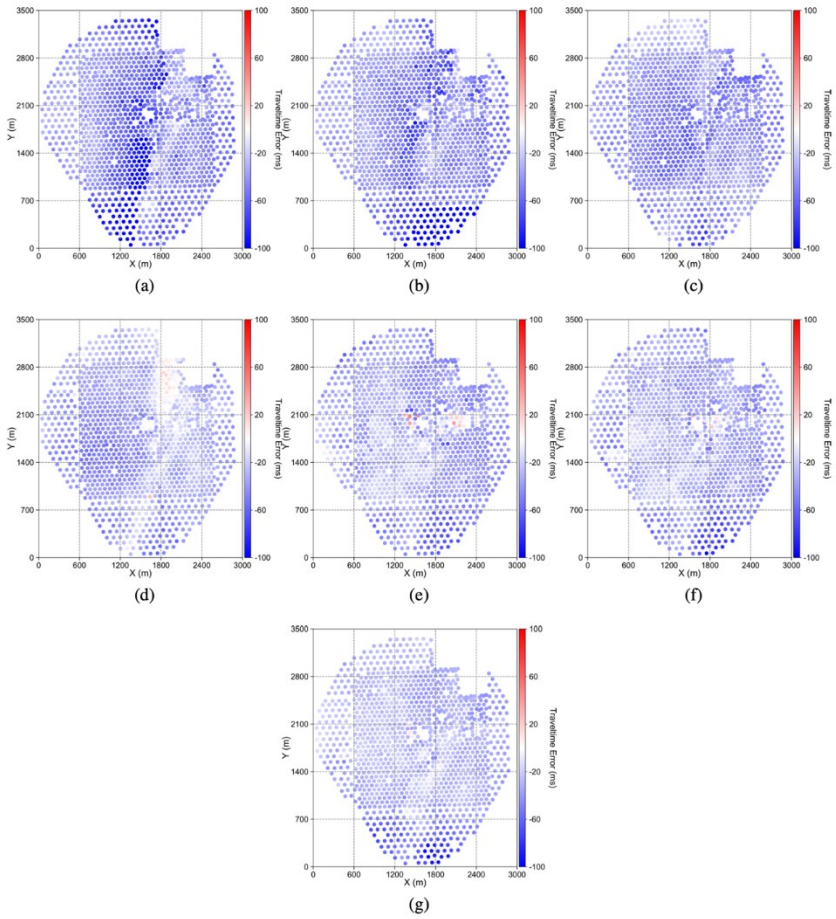

Figure 7: Panels (a)-(g) display the misfit between the computed first-arrival traveltimes and the observed first-arrival traveltimes in the initial velocity model.

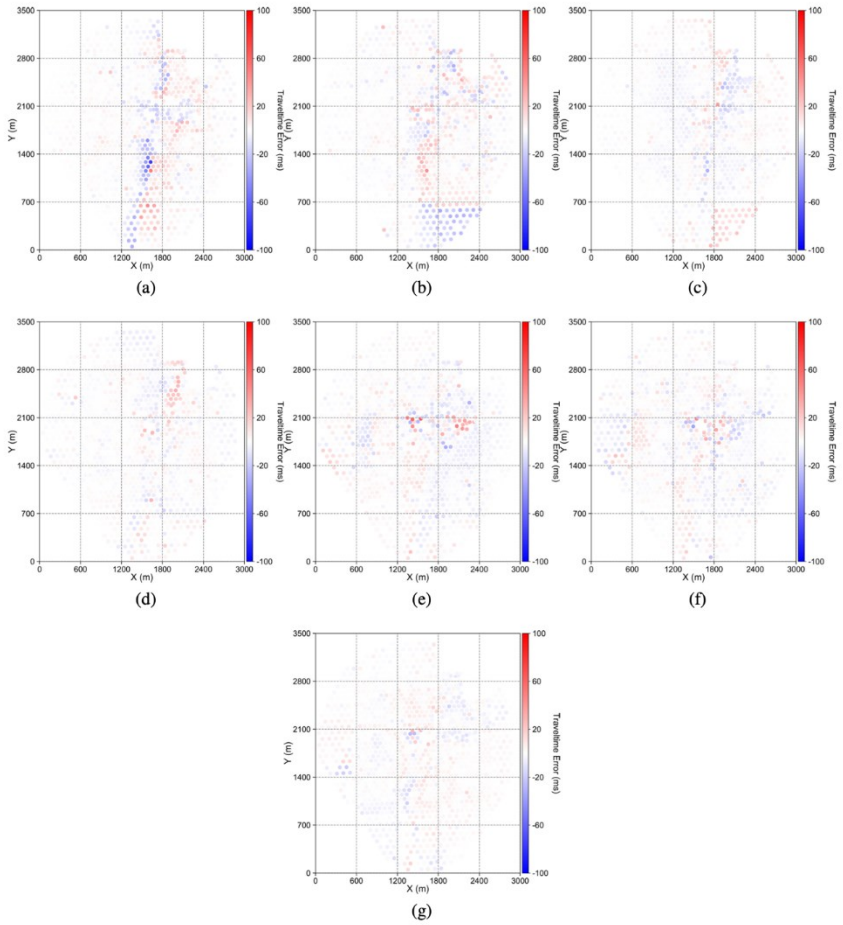

Figure 8: Panels (a)-(g) display the misfit between the computed first-arrival traveltimes and the observed first-arrival traveltimes in our FATT-inverted velocity model.

With the original and the updated velocity models, we perform two sets of cross-coherence passive seismic migration described in the Methodology section using the continuously recorded seismic data.

Each passive seismic dataset contains 24-hour continuous waveforms recorded at the 1,206 large-N nodal geophones, spanning from Julian day 214 to day 230, 2020. The data are divided into one-minute segments for each station to accommodate SEG-Y storage of the data. The data were corrected to the reference datum but were not bandpass filtered, so the frequency contents are completely preserved for LPLD study. Figures 9-10 display the first 110 traces of an example dataset of day 214 where the left panels show the waveforms and the right panels display the spectrograms of two different traces. It is evident that the waveforms are complex and vary in their time-frequency characteristics in different traces. For some traces, the spectrogram spans almost the entire frequency band, indicating that the recorded waveforms are mostly ambient noises. For the other traces, we observe notable energy concentration at a certain frequency range and at a certain time range, indicating that they are either coherent environmental noises (power plant operation, vehicles, winds, etc.) or passive seismic signals associated with unknown events that were not captured at all stations. This inconsistency at different nodal geophones complicates the imaging process because it effectively results in notable sparsification of the observational system, i.e., only a few (sparsely-distributed) nodal geophones recorded useful microseismic data.

For the cross-coherence seismic migration, we choose the continuous seismic data recorded from 00:00 to 05:00 each day, because the level of environmental noises during this time period each day is lower compared with other time, and therefore, it is easier and more feasible to use these signals to produce reliable images of geothermal fluid flow activities and flow pathways.

Figures 11 and 12 display the 3D slice views of the source images for Julian day 214 of 2020 (i.e., August 2, 2020) obtained using the original and our FATT-updated velocity models, respectively. The blue to red colors on these images represent the amplitudes of source images, i.e., the degree of geothermal flow activities within the fracture system. The red colors indicate higher flow rate or stronger fracture expansion/contraction. Comparing these two source images, particularly the horizontal slices of these images, we find that in both original and updated velocity models, the region around the two production wells (the red tubes in the 3D plots) shows the most active geothermal flow activity. The source image produced using the cross-coherence migration in the FATT-updated velocity model (Figure 12) displays higher spatial resolution compared with that obtained using the original velocity model (Figure 11). The comparison indicates that an accurate velocity model is crucial to produce high-resolution geothermal flow images.

We perform the same cross-coherence migration procedure for the continuous seismic data of other days (Julian days 214 to 226) using both original and our updated velocity models, and display the imaging results for days 218, 222, and 226 in Figures 13/14, Figures 15/16, and Figures 17/18, respectively. Similar to the imaging results for day 214, the images obtained using the updated velocity model are of higher spatial resolution compared with those produced using the original smooth velocity model. The results indicate again that, for reliable passive seismic imaging, it is crucial to use highly-accurate medium property models.

We also find that the source images on different days vary in their spatial patterns. For example, the LDG power plant was shut down during August 2 to 4 (Julian days 214 to 216), 2020, and returned to normal operations on August 10 (Julian day 222), 2020. Comparing the source image of day 222 (Figure 16) and day 214 (Figure 12), we find that the energy source of LPLD signals on day 222 is more concentrated around the production well. A more reliable time-lapse analysis of the geothermal fluid flow activities within the geothermal fracture system at the LDG resource area using this passive seismic imaging approach may require a more careful treatment of the absolute amplitude during the imaging process. Currently, the deconvolution operation adopted by the cross-coherence imaging condition modifies, or more precisely, normalizes the amplitude of input passive seismic signals, and therefore, leads to difficulties in providing properly-scaled amplitudes of source images on different days.

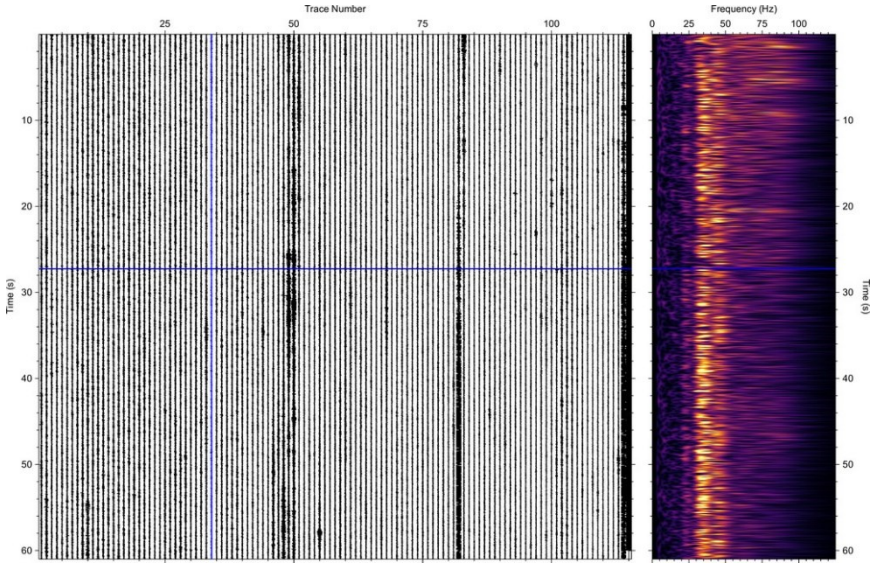

Figure 9: Trace plot (left) and the spectrogram of one of the traces marked by the vertical blue line (right) for one minute of the continuous data.

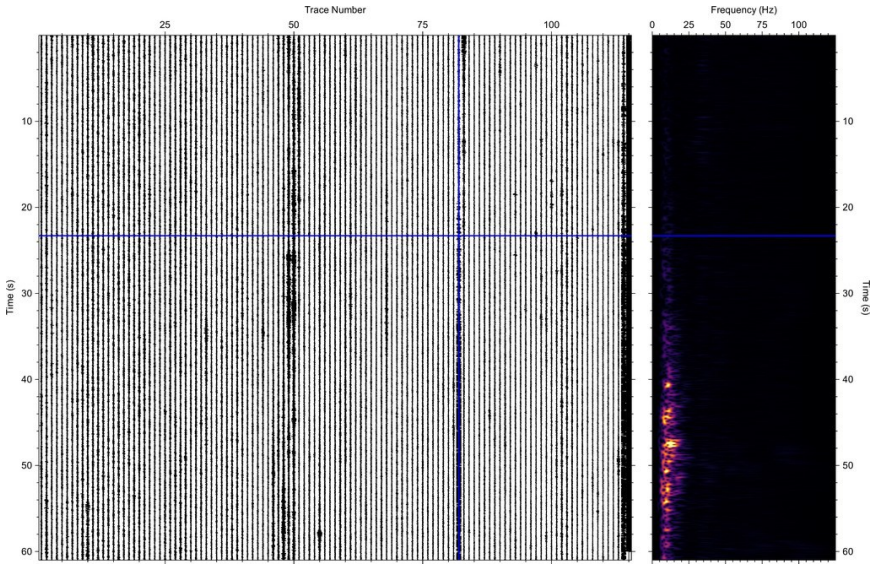

Figure 10: Trace plot (left) and the spectrogram of one of the traces marked by the vertical blue line (right) for one minute of the continuous data.

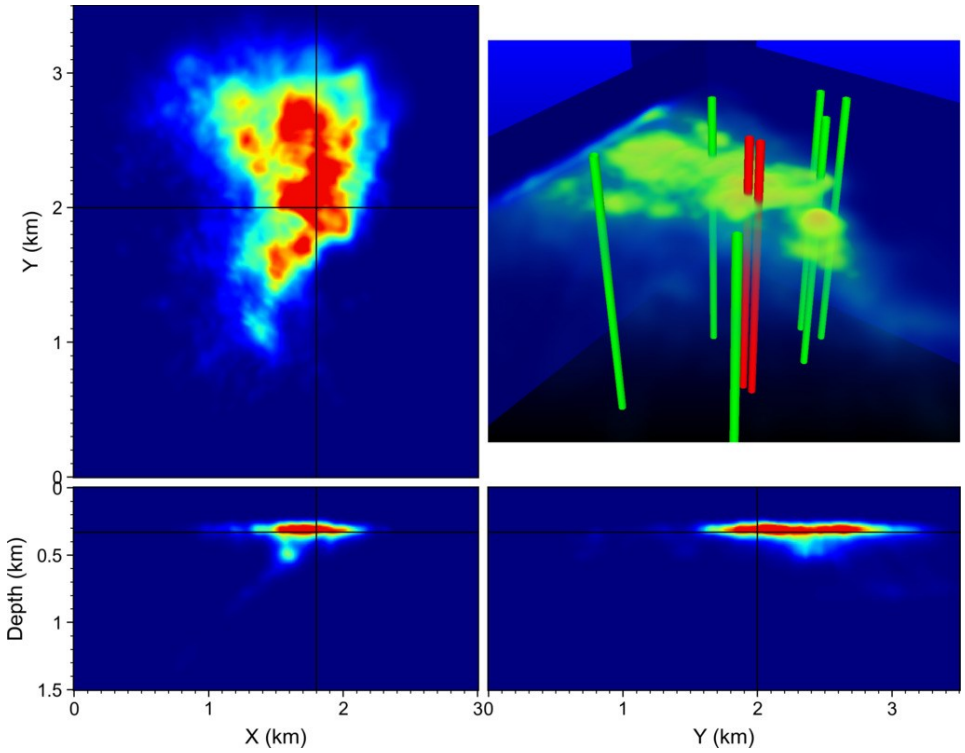

Figure 11: Source image of LPLD signals obtained using the original Vp model for Day 214.

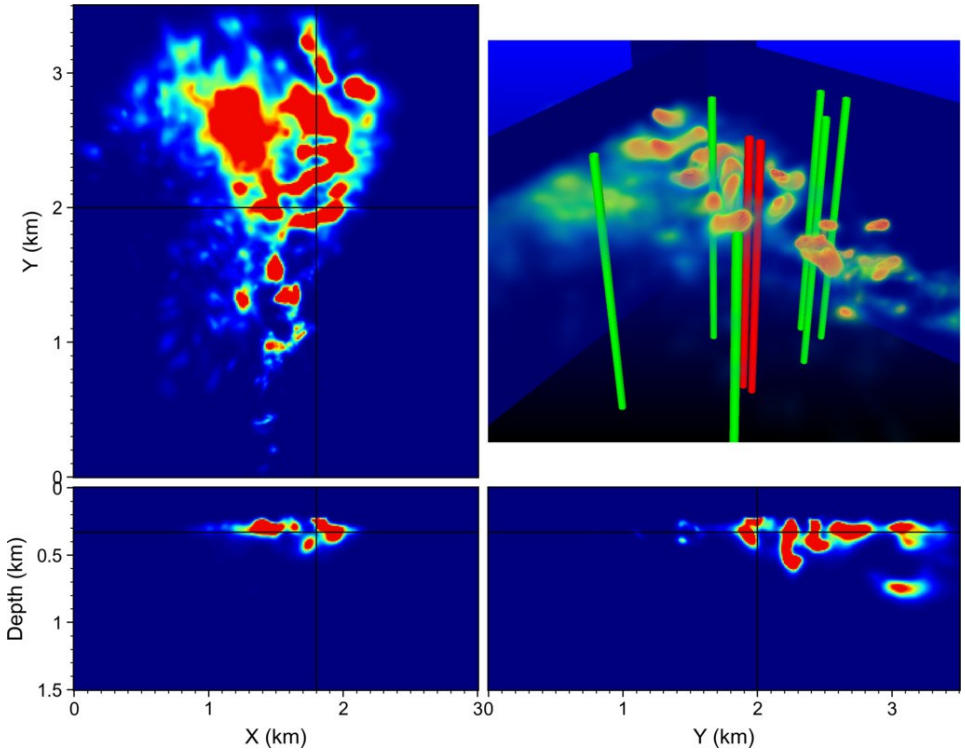

Figure 12: Source image of LPLD signals obtained using the FATT-updated Vp model for Day 214.

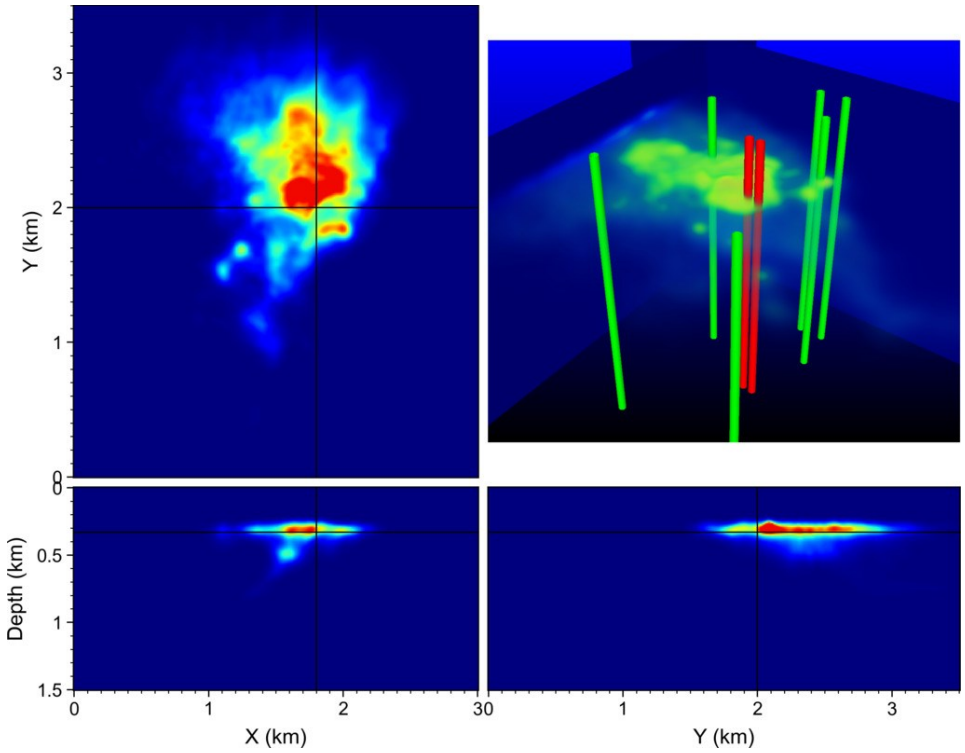

Figure 13: Source image of LPLD signals obtained using the original Vp model for Day 218.

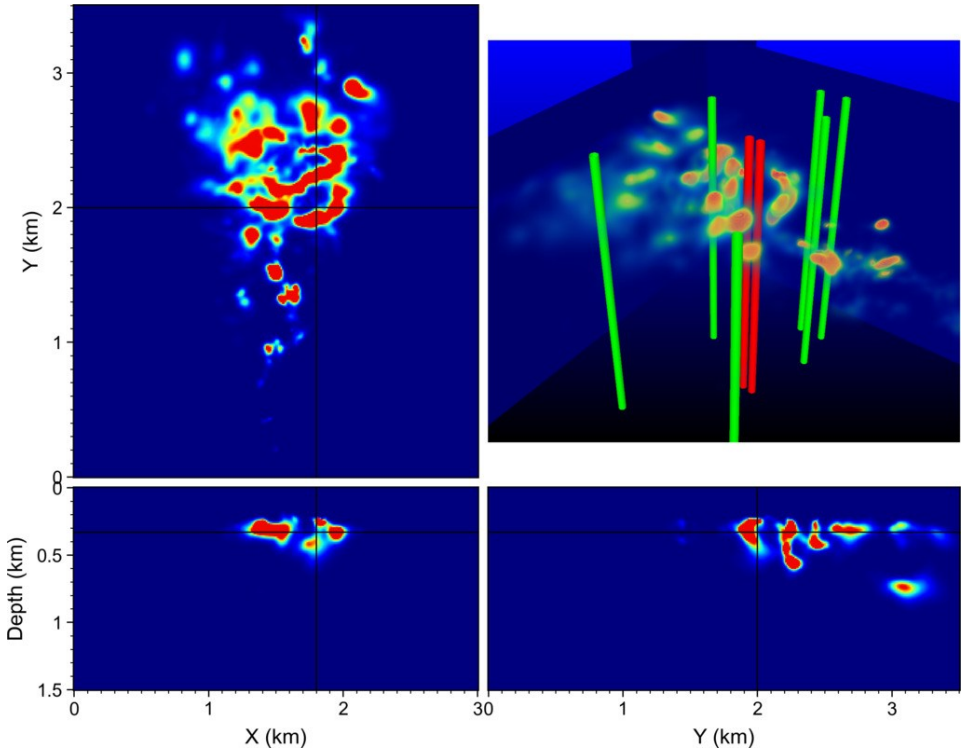

Figure 14: Source image of LPLD signals obtained using the FATT-updated Vp model for Day 218.

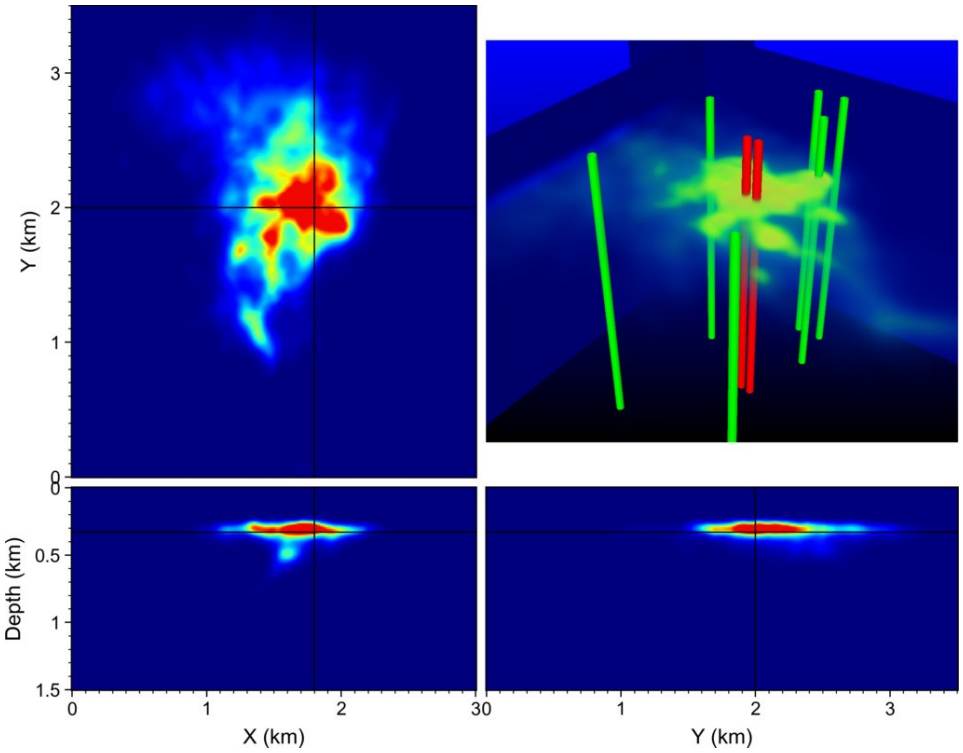

Figure 15: Source image of LPLD signals obtained using the original Vp model for Day 222.

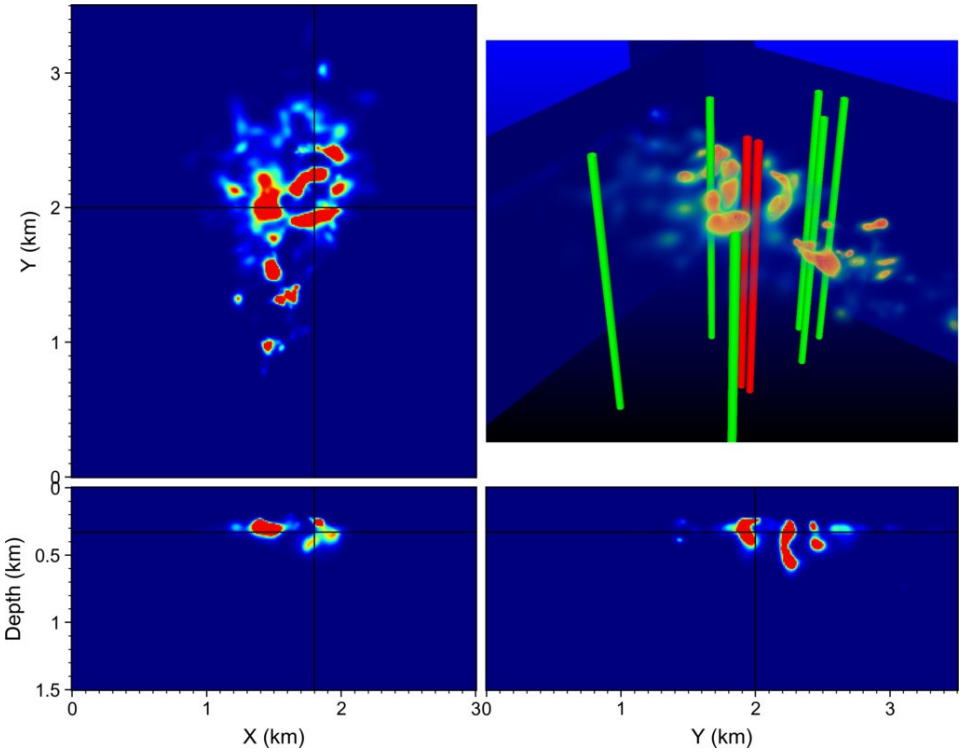

Figure 16: Source image of LPLD signals obtained using the FATT-updated Vp model for Day 222.

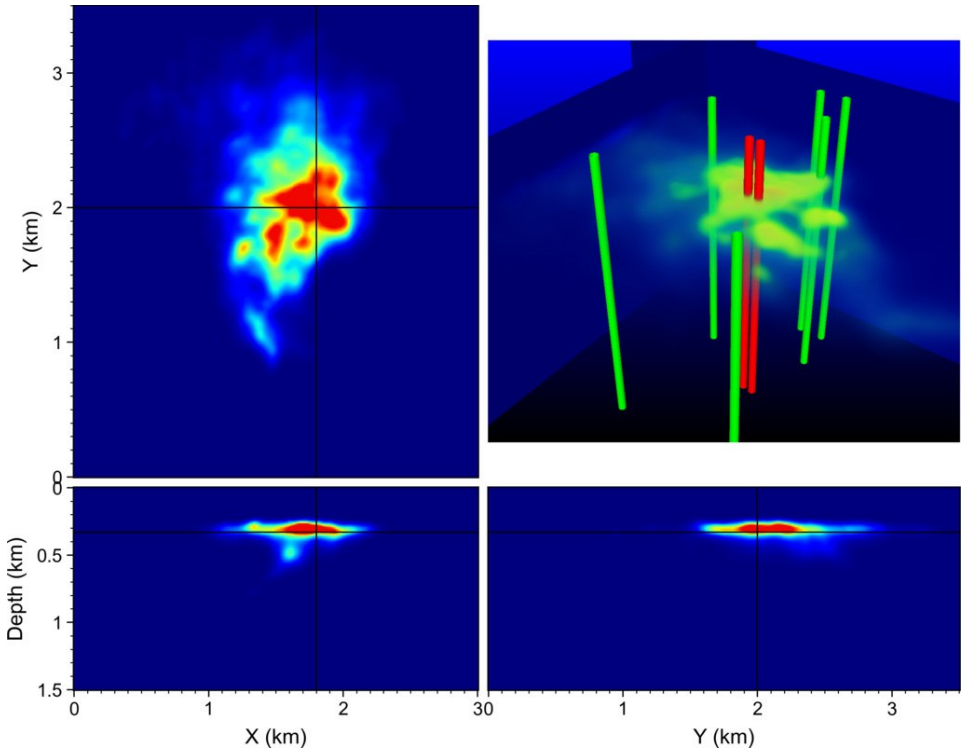

Figure 17: Source image of LPLD signals obtained using the original Vp model for Day 226.

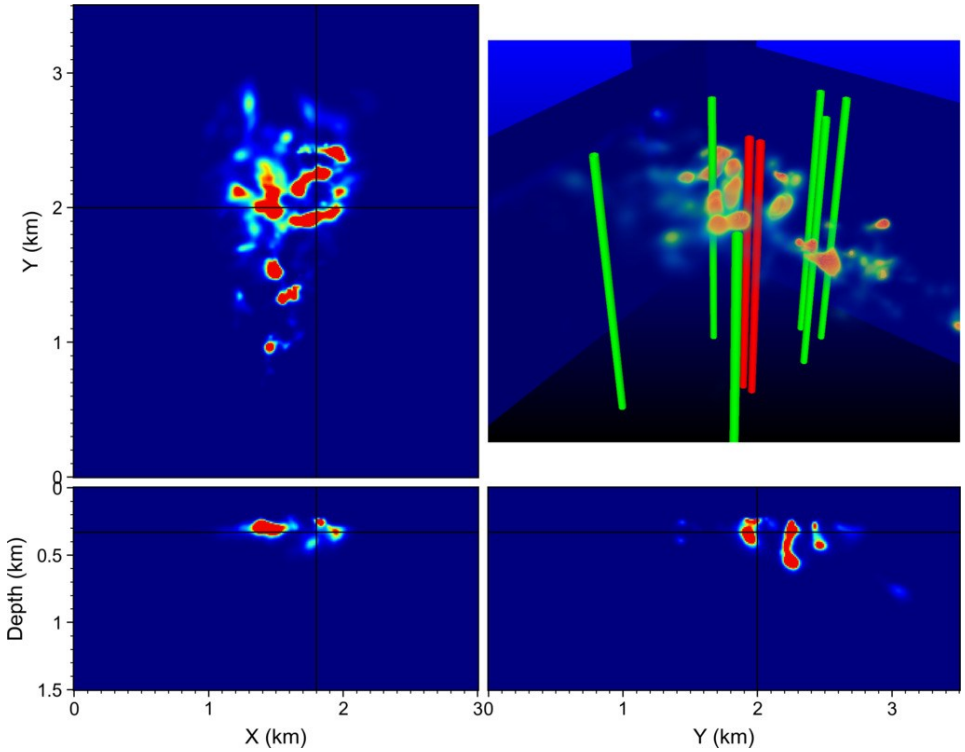

Figure 18: Source image of LPLD signals obtained using the FATT-updated Vp model for Day 226.

4. CONCLUSIONS

We have performed an adjoint-state first-arrival traveltime tomography (FATT) using active seismic data acquired with seven borehole string shots and a large-N array consisting of 1,206 nodal geophones to update the initial velocity model at the Lightning Dock geothermal resource area. With the updated velocity model, we have performed geothermal fluid flow imaging using frequency-domain cross-coherence passive seismic migration of the continuously-recorded long-duration, long-period passive seismic data acquired using the large-N array at the Lightning Dock geothermal resource area. Our imaging results reveal the spatial-temporal geothermal fluid flow activities and associated geothermal fracture pathways within the Lightning Dock geothermal reservoir. These imaging results provide valuable information for siting new geothermal wells and increase geothermal production.

ACKNOWLEDGMENTS

This work was supported by The New Mexico Small Business Assistance (NMSBA) Program. This research used resources provided by the LANL Institutional Computing Program, which is supported by the U.S. DOE NNSA under Contract No. 89233218CNA000001.

REFERENCES

Artman, B., I. Podladtchikov, and B. Witten, 2010, Source location using time-reverse imaging: Geophysical Prospecting, 58, no. 5, 861–873, doi: 10.1111/j.1365-2478.2010.00911.x.

Das, I., and M. D. Zoback, 2013, Long-period, long-duration seismic events during hydraulic stimulation of shale and tight-gas reservoirs – Part 1: Waveform characteristics: Geophysics, 78, no. 6, KS97–KS108, doi: 10.1190/geo2013-0164.1.

Leung, S., and J. Qian, 2006, An adjoint state method for three-dimensional transmission traveltime tomography using first-arrivals: Communications in Mathematical Sciences, 4, no. 1, 249–266.

Liu, Y., Y. Ma, and Y. Luo, 2020, Source location with cross-coherence migration: Geophysics, 85, no. 4, KS127–KS138, doi: 10.1190/geo2019-0311.1.

Sirgue, L., J. Etgen, and U. Albertin, 2008, 3D frequency domain waveform inversion using time domain finite difference methods: Expanded Abstracts of 70th EAGE Conference & Exhibition, Rome, Italy.

Taillandier, C., M. Noble, H. Chauris, and H. Calandra, 2009, First-arrival traveltime tomography based on the adjoint-state method: Geophysics, 74, no. 6, WCB1–WCB10, doi: 10.1190/1.3250266.

Yukutake, Y., R. Honda, M. Harada, R. Doke, T. Saito, T. Ueno, S. Sakai, and Y. Morita, 2017, Analyzing the continuous volcanic tremors detected during the 2015 phreatic eruption of the Hakone volcano: Earth, Planets and Space, 69, no. 1, 164, doi: 10.1186/s40623-017-0751-y.

Zanskar, 2021, Passive seismic survey over the Lightning Dock Geothermal Area, Hidalgo County, New Mexico: Confidential Internal Project Report.